Numerical Feasibility Analysis of an Epidermal Glucose Sensor based on Time-Resolved Fluorescence

Kamal M. Katika and Laurent Pilon

Mechanical and Aerospace Engineering Department, Henri Samueli School of Engineering and Applied Science, University of California, Los Angeles, Los Angeles, CA 90095;

ABSTRACT

This paper presents numerical simulations predicting the time-resolved reflectance and autofluorescence of human skin exposed to a pulse of collimated light at 337 nm and pulse width of 1 ns. Moreover, the feasibility of using an embedded time-resolved fluorescence sensor for monitoring glucose concentration is also studied. Skin is modeled as a multilayer medium with each layer having its own optical properties and fluorophore absorption coefficients, lifetimes and quantum yields. The intensity distributions of excitation and fluorescent light in skin are then determined by solving the transient radiative transfer equation using the modified method of characteristics. In both cases, the fluorophore lifetimes are recovered from the simulated fluorescence decays and compared with the actual lifetimes used in the simulations. It was found that the fluorescence lifetime of the fluorophore contributing the least to the fluorescence signal could not be recovered while the other lifetimes could be recovered within 2.5% of input values. Such simulations could be valuable in interpreting data from time-resolved fluorescence experiments on healthy and diseased tissue as well as in designing and testing the feasibility of various optical sensors for biomedical diagnostics.

Keywords: time-resolved fluorescence, method of characteristics, skin optics, turbid media, diabetes, non-invasive glucose monitoring, human skin

1. INTRODUCTION

Biological tissues contain several endogenous fluorophores such as NADH, aromatic amino acids like tryptophan and structural proteins such as collagen and elastin [1]. Moreover, exogeneous fluorescing substances can be applied onto the skin or implanted within. The properties of these fluorophores are sensitive to the environment and the metabolic status of the tissue thus, making fluorescence spectroscopy an attractive tool to study the health of biological tissues. For example, implantable fluorescent sensors have been proposed for non-invasive monitoring of glucose concentrations in diabetic individuals [2,3]. These sensors consist of a layer of fluorescent microspheres made out of a polymer hydrogel implanted in the skin between the epidermis and dermis, for example. The fluorescence intensity emitted by these fluorophores is sensitive to glucose concentrations and thus the interstitial fluid glucose concentrations can be monitored [4]. However, intensity based measurements are sensitive to fluorophore concentration and to the intensity of the fluorescence signal [5]. On the other hand, fluorescence lifetimes are independent of fluorophore concentration and the fluorescence intensity. DiCesare *et al.* [5] have synthesized fluorescence probes whose lifetimes are sensitive to the concentrations of glucose *in-vitro* [5].

Practically, fluorescence spectroscopy techniques consist of exposing the tissue of interest to excitation light (typically UV) and measuring the fluorescence emission spectrum. The incident excitation can be a continuous or an ultra-short pulse beam of UV light. It can also be collimated or diffuse whether a laser or a diffuse source is used. These measurements can be carried out in a steady-state or time-resolved manner. In either case, the fluorophores are present throughout the tissue and the excitation and fluorescent light is absorbed and scattered by tissue before emerging and reaching the detector. Thus, the fluorescence measurements strongly depend on the tissue's optical properties and morphology. In order to capture these effects, as well as those of the geometry of the optical setup, an accurate model of excitation and fluorescent light transport in tissue is needed.

Further author information:(Send correspondence to Laurent Pilon.)
Kamal M. Katika: E-mail: kamal@seas.ucla.edu
Laurent Pilon: E-mail: pilon@seas.ucla.edu

The first objective of the present work is to develop an optical model and computer program simulating the time-resolved fluorescence from human skin. The second is to test the feasibility a sensor, based on time-resolved fluorescence, and implanted under the skin for non-invasively monitoring glucose concentrations.

2. CURRENT STATE OF KNOWLEDGE

Both experimental and numerical studies have been performed for time-resolved fluorescence measurements in turbid media and tissue. The reader is referred to Ref. [1] and references therein for experimental studies on time-resolved fluorescence. This review section is limited to numerical studies of light transport and fluorescence in tissue.

One of the most common numerical tools used to study reflectance and fluorescence in biological tissue is the Monte Carlo method [6–9]. It is a statistical method consisting of tracing the history of a statistically meaningful number of photons from their points of emission to their points of absorption [10]. The main advantage of the Monte Carlo method resides in its simplicity and ability to deal with complex problems with relative ease. However, it requires a statistically meaningful number of photons and hence can be time consuming. The Monte Carlo technique has been used by Vishwanath *et al.* [11] to simulate time-resolved fluorescence from semi-infinite homogeneous turbid media. It was shown that the recovered lifetimes increased with increasing scattering and source-detector distance. This increase in lifetime was in good agreement with those seen in experiments performed by the same authors. They then applied the Monte Carlo technique [12] to model data obtained from clinical measurements in the lower gastro-intestinal tract. They investigated the effects of various parameters such as the tissue thickness, quantum yield, and absorption coefficients of the tissue on the fluorescence decay curves obtained. In addition, Vishwanath and Mycek [13] showed numerically that fluorescence lifetime measurements can be affected significantly in semi-infinite and inhomogeneous turbid media by fluorophore properties other than intrinsic lifetimes such as fluorophore spatial distribution and concentration. Significant variations in the recovered average lifetimes were observed by changing the tissue morphology or factors related to tissue biochemistry in the numerical simulations while keeping the fluorescence lifetimes constant. These variations were comparable to the differences seen in the average lifetimes obtained from experiments on normal tissue and adenomatous polyps [13].

Alternatively, the diffusion approximation has been used by researchers to simulate transient fluorescence transport in turbid media. For example, Patterson and Pogue [14] have used it to predict the fluorescence photon fluence rate from semi-infinite tissue. The diffusion approximation was also used by Leary *et al.* [15] and Muraca and co-workers [16, 17] for fluorescence lifetime imaging in two-dimensional turbid media. While the diffusion approximation has been widely used to simulate radiation transport in biological tissue, it cannot be applied to all types of tissue. Indeed, in a comparison between the diffusion approximation and the radiative transfer equation (RTE) [10], Hielscher *et al.* [18] have shown that the diffusion approximation fails to predict the steady-state fluence accurately for tissues with very low scattering and absorption coefficients. The diffusion approximation also gives inaccurate results in highly absorbing tissue [18]. Moreover, its validity for transient light transport in heterogeneous biological tissues with non-scattering or low-scattering regions has been questioned [19]. Indeed, Elaloufi *et al.* [19] have shown that the diffusion approximation fails to describe both short-time and long-time transmittance of optically thin slabs for both weakly and strongly absorbing media. In the case of optically thick slabs, the diffusion approximation fails for short times. This issue has also been discussed by Guo and Kim [20] in the transport of ultra-fast laser pulses in biological tissues. In addition, it is difficult to describe collimated sources using the diffusion approximation without carefully choosing the source terms [21]. Moreover, Yoon *et al.* [22] compared the steady-state diffusion approximation with the solution of the steady-state RTE using the discrete ordinates method for a 1-D absorbing and scattering slab illuminated by a collimated beam of light. Various quantities such as the diffuse intensity (or radiance), total fluence, and diffuse flux were computed. The effect of the optical transport coefficients such as the single scattering albedo and the scattering anisotropy factor on the accuracy was also studied. The authors concluded that the diffusion approximation does not yield accurate angular profiles of the intensity except at locations far from the source and the boundaries [22]. Furthermore, they showed that the diffusion approximation estimates low reflection and high transmission for forward scattering and is not recommended for a highly anisotropically scattering medium [22].

As mentioned earlier, there has been a rising interest in non-invasive glucose sensors based on fluorescence. Currently, diabetic patients measure their blood glucose concentrations by finger-prick capillary blood sampling, which is painful and prevents detection of abnormal glucose levels while sleeping or driving. Therefore, a non-invasive and continuous glucose sensing is a priority in diabetes care [23]. Moreover, skin is the most accessible organ in the human body allowing for non-invasive sensing and convenient continuous monitoring. In the present paper, the feasibility of using implantable sensors for *in-vivo* monitoring glucose concentrations using time-resolved fluorescence is studied. First, a model of skin fluorophores is constructed using numerical and experimental data available in literature. The hemispherical time-resolved fluorescence from human skin is then obtained by solving the radiative transfer equation using the modified method of characteristics [24, 25]. Next, the fluorescence lifetimes are recovered from these decays using Fluofit [26, 27] and compared with the actual lifetimes of the fluorophores used in the simulations. Finally, the time-resolved fluorescence from skin with an implanted glucose sensor is simulated and fluorescence lifetimes recovered. An attempt is then made to determine the glucose concentrations based on the recovered fluorescence lifetimes. To the best of our knowledge, these simulations represent the first attempt to model time-resolved fluorescence from human skin using the radiative transfer equation. Moreover, it presents the first numerical feasibility study of implanted sensors based on time-resolved fluorescence.

3. ANALYSIS

3.1. Skin Morphology

Skin is a complex biological structure made of different layers with different morphologies and optical properties. The topmost layer of the skin is the so-called *stratum corneum* and composed of mainly dead cells embedded in a lipid matrix. The layer below is the *epidermis* and consists of cells containing keratohyalin granules, columnar cells, and other cells containing melanosomes and small melanin granules [28]. The third major layer of the skin is called the *dermis* and is primarily made up of collagen fibers with nerves and blood vessels running through. The *dermis* is sometimes divided into the *papillary dermis* and the *reticular dermis* based on the size of the blood vessels in them [29]. All these layers add up to a thickness of about 2 mm [30]. Finally, there is the subcutaneous layer beneath the dermis which consists of fat [8].

Let us consider an area of skin exposed to monochromatic excitation light with wavelength λ_x. The excitation source could be a UV flash lamp or an ultra-short pulse laser or a light emitting diode (LED). The excitation light as it travels through the skin is then scattered or absorbed. Moreover, some absorbers such as proteins in the skin are known to fluoresce when excited at particular wavelengths. When a fluorescense based sensor is embedded between the epidermis and the dermis, it will contribute to the overall absorption, scattering and fluorescence from the skin. The fluorescence from the skin and the sensor can be transported to a detector by means of a strategically placed optical guide. If one assumes that the field of illumination is wider than the skin thickness, the problem can be treated as one-dimensional. Figure 1 shows the skin morphology and the excitation and detection configuration adopted in the present study.

3.2. Governing Equations

The governing equation describing the transport of light in skin is the transient radiative transfer equation (RTE). Even though it is a complex integro-differential equation involving seven variables, it is preferred to the diffusion approximation for the reasons discussed previously. For an absorbing, scattering and non-emitting media, the RTE can be expressed as [10],

$$\frac{1}{c_{\lambda_x}}\frac{\partial I_{\lambda_x}(\mathbf{r},\hat{\mathbf{s}},t)}{\partial t} + (\hat{\mathbf{s}}\cdot\nabla)I_{\lambda_x}(\mathbf{r},\hat{\mathbf{s}},t) = -\kappa_{\lambda_x}I_{\lambda_x}(\mathbf{r},\hat{\mathbf{s}},t) - \sigma_{s,\lambda_x}I_{\lambda_x}(\mathbf{r},\hat{\mathbf{s}},t) +$$

$$\frac{\sigma_{s,\lambda_x}}{4\pi}\int_{4\pi}I_{\lambda_x}(\mathbf{r},\hat{\mathbf{s}}_i,t)\Phi_{\lambda_x}(\hat{\mathbf{s}}_i,\hat{\mathbf{s}})\mathrm{d}\Omega_i \quad (1)$$

where $I_{\lambda_x}(\mathbf{r},\hat{\mathbf{s}},t)$ is the excitation intensity at wavelength λ_x in direction $\hat{\mathbf{s}}$ at location $\mathbf{r}$ and time t, κ_{λ_x} and σ_{s,λ_x} are the linear absorption and scattering coefficients at the excitation wavelength, respectively. The scattering phase function $\Phi_{\lambda_x}(\hat{\mathbf{s}}_i,\hat{\mathbf{s}})$ represents the probability that radiation propagating in the solid angle $d\Omega_i$ around
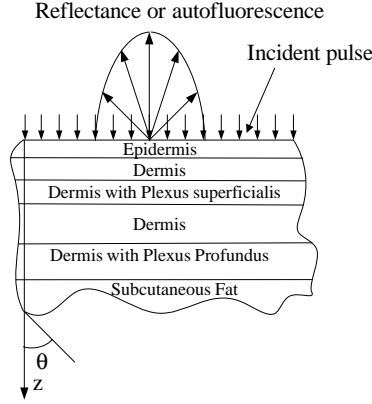
Figure 1. Geometry of excitation and detection of reflectance and autofluorescence used in the simulations.

direction $\hat{\mathbf{s}}_i$ be scattered into the solid angle $d\Omega$ around direction $\hat{\mathbf{s}}$. The speed of light in the medium at the excitation wavelength is denoted c_{λ_x}. The first and second terms on the right-hand side represent attenuation of the radiation intensity by absorption and scattering, respectively. The last term corresponds to the augmentation of radiation due to in-scattering. Note that here, the emission by the skin at $37°C$ at the excitation wavelength λ_x is negligible compared with the excitation intensity.

Moreover, a similar equation can be written for the transport of the fluorescent light emitted by the fluorophores at wavelength λ_F [1, 31]

$$\frac{1}{c_{\lambda_F}}\frac{\partial I_{\lambda_F}(\mathbf{r},\hat{\mathbf{s}},t)}{\partial t} + (\hat{\mathbf{s}}\cdot\nabla)I_{\lambda_F}(\mathbf{r},\hat{\mathbf{s}},t) = -\kappa_{\lambda_F}I_{\lambda_F}(\mathbf{r},\hat{\mathbf{s}},t) - \sigma_{s\lambda_F}I_{\lambda_F}(\mathbf{r},\hat{\mathbf{s}},t) +$$

$$\frac{\sigma_{s\lambda_F}}{4\pi}\int_{4\pi}I_{\lambda_F}(\mathbf{r},\hat{\mathbf{s}}_i,t)\Phi_{\lambda_F}(\hat{\mathbf{s}}_i,\hat{\mathbf{s}})d\Omega_i + \frac{QY_{\lambda_x}\kappa_{\lambda_{xF}}}{4\pi\tau_{\lambda_x}}\int_0^t exp\left[-\left(\frac{t-t'}{\tau_{\lambda_x}}\right)\right]G_{\lambda_x}(\mathbf{r},t')dt' \quad (2)$$

The last term in Equation (2) represents the fluorescence emission by the fluorophores and $G_{\lambda_x}(\mathbf{r},t)$ is the excitation light fluence at location $\mathbf{r}$ and time t and is defined as $G_{\lambda_x}(\mathbf{r},t) = \int_{4\pi}I_{\lambda_x}(\mathbf{r},\hat{\mathbf{s}},t)d\Omega$. The quantum yield of the fluorophores is denoted by QY_{λ_x}, while $\kappa_{\lambda_{xF}}$ is the absorption coefficient of the fluorophores at the excitation wavelength λ_x and τ_{λ_x} denotes the lifetime of the fluorophores.

Finally, for both excitation and emission wavelengths, the Henyey-Greenstein phase function was used to account for the anisotropic nature of scattering by each layer of the skin and is expressed as,

$$\Phi_\lambda(\Theta) = \frac{1-g_\lambda^2}{[1+g_\lambda^2-2g_\lambda\cos\Theta]^{3/2}} \quad (3)$$

where, g_λ is the spectral scattering asymmetry factor and Θ is the angle between the incident direction $\hat{\mathbf{s}}_i$ and the scattering direction $\hat{\mathbf{s}}$.

3.3. Closure Laws

In order to solve the above equations, one needs (i) a model of the skin morphology, (ii) the optical and radiation characteristics c_λ, κ_λ, $\sigma_{s\lambda}$, Φ_λ of the skin layers at the excitation and emission wavelengths, and (iii) the spatial distribution of the fluorophores, and (iv) their quantum yields QY_{λ_x}, (v) their lifetimes τ_{λ_x}, and (vi) their absorption coefficients $\kappa_{\lambda_{xF}}$. Various optical models have been used to study light transport in skin [30, 32, 33], each varying in complexity. In the present study, the optical model of human skin developed by Tuchin *et al.* [30] was chosen for its relative simplicity while capturing enough detail of the skin morphology. It consists of five

plane-parallel layers, corresponding to (1) the epidermis, (2) the dermis, (3) the dermis with *plexus superficialis*, (4) the dermis, and (5) the dermis with *plexus profundus*. The thicknesses and optical properties of these layers at wavelengths 337 and 577 nm are reproduced in Table 1. Furthermore, in spite of varying refractive indices within the skin, reflection and refraction effects at the interfaces between the skin layers are considered negligible as the difference in refractive index between these layers is very small (see Table 1). Instead, only the speed of light, $c_\lambda = c_0/n_\lambda$ used in Equations (1) and (2) was varied in each layer. Had there been a larger change in the refractive indices between adjacent layers, then the RTE would have had to be solved in each layer separately with the appropriate boundary conditions.

Furthermore, the distribution of fluorophores in the skin was based on studies reported in the literature [34,35]. According to Gillies *et al.* [35], the fluorescence from skin when excited at a wavelength of 337 nm is mainly from collagen present in the dermis. Moreover, Koenig and Riemann [35] also reported the presence of NADH in human skin in the epidermis at a depth of 50 μm from the surface. Using this information, a model of fluorophore distribution within the skin was developed in which the sources of fluorescence from the skin were NADH in the epidermis (layer 1) and collagen in all the other layers. In addition, the quantum yield, lifetime and absorption coefficients of these fluorophores at around 337 nm and 577 nm were obtained from the literature [12, 13]. It should be noted that there are other endogenous fluorophores present in the skin such as lipofuscin which is excited in the UV/visible region and emits at around 570 to 590 nm [35]. These fluorophores were not taken into account here for the sake of simplicity. Finally, the *in-vitro* emission maxima of NADH and collagen when excited at 337 nm are close to 450 and 390 nm, respectively [1]. However, their fluorescence at 577 nm is studied here due to the fact that properties of skin at this wavelength were readily available in literature [30]. Moreover, there have also been numerical and experimental studies of the time-resolved fluorescence from colon tissue at an emission wavelength of 550±20 nm with NADH and collagen as the principal fluorophores [12,13]. This indicates that even though the chosen emission wavelength of 577 nm is different from the emission maxima of NADH and collagen, their fluorescence can still be observed *in-vivo* at this wavelength.

Table 1. Optical properties used in the five-layer skin model, here $\lambda_x = 337$ nm and $\lambda_F = 577$ nm. [13,30].

Layer	$Thickness^*$	n^*		κ_λ^* (cm^{-1})		$\sigma_{s,\lambda}^*$ (cm^{-1})		g_λ^*		$\tau_{\lambda_x}^+$ (ns)	$\kappa_{\lambda_{xF}}^+$ (cm^{-1})	$QY_{\lambda_x}^+$
	μm	λ_x	λ_F	λ_x	λ_F	λ_x	λ_F	λ_x	λ_F	$\sim \lambda_x$	$\sim \lambda_x$	$\sim \lambda_x$
Epidermis	100	1.5	1.5	32	10.7	165	120	0.72	0.78	1.5	3.15	0.05
Dermis	200	1.4	1.4	23	3	227	205	0.72	0.78	5.2	0.9	0.3
Dermis with plexus superficialis	200	1.4	1.4	40	5.2	246	219	0.72	0.78	5.2	0.9	0.3
Dermis	900	1.4	1.4	23	3	227	205	0.72	0.78	5.2	0.9	0.3
Dermis with plexus profundus	600	1.4	1.4	46	6	253	225	0.72	0.78	5.2	0.9	0.3

+ from Ref. [13],* from Ref. [30]

Moreover, several simplifying assumptions are made to model the fluorescence from the embedded glucose sensor. The glucose sensor is assumed to be a homogeneous absorbing and scattering plane-parallel slab of thickness 50 μm with uniformly distributed fluorophores. The fluorophore is assumed to be 9-[[N-Methyl-N-(o-boronobenzyl) amino]methyl]anthracene whose fluorescence lifetimes change as a function of glucose concentration [5]. The mean fluorescence lifetime of this compound at an excitation wavelength of 370 nm and an emission wavelength of 420 nm is 11.25 ns at a glucose concentration of 5mM [5] which is close to the normal blood glucose level of 5.55 mM [36]. The fluorophore layer is assigned optical properties from the fluorescence layer described in Ref. [3]. Here the fluorophore was arbitrarily assigned a quantum yield and absorption coefficient of fluorescein while the scattering coefficient was determined by assuming that the layer was a translucent gel polymer largely composed of water. These parameters can however be varied depending on the polymer material and the fluorophore selected. Furthermore, the skin model was simplified considerably to reduce the computational time. In the new model, skin was assumed to be made up of only two layers, the epidermis and

the dermis. While the optical properties of the epidermis were retained from the previous model, the optical properties of the dermis were obtained by averaging of the optical properties of the layers below the epidermis in the previous model. For example, the average absorption coefficient at the excitation wavelength is given by $\kappa_{\lambda_x} = \sum_i \kappa_{\lambda_x i} L_i / \sum_i L_i$, where L_i is the thickness of each layer i. This can be justified by the fact that these properties do not vary significantly from one layer to another in the dermis. Table 2 lists the optical properties of the two-layer skin model along with those of the embedded sensor layer.

Table 2. Optical properties of the simplified two-layer skin model with an embedded glucose sensor, here $\lambda_x = 337$ nm and $\lambda_F = 577$ nm.

Layer	Thickness	n		κ_λ (cm^{-1})		$\sigma_{s,\lambda}$ (cm^{-1})		g_λ		τ_{λ_x} (ns)	$\kappa_{\lambda_{xF}}$ (cm^{-1})	QY_{λ_x}
	μm	λ_x	λ_F	λ_x	λ_F	λ_x	λ_F	λ_x	λ_F	$\sim \lambda_x$	$\sim \lambda_x$	$\sim \lambda_x$
Epidermis	100	1.5	1.5	32	10.7	165	120	0.72	0.78	1.5	3.15	0.05
Sensor	50	1.37	1.37	1.88	0.1	10	10	0.9	0.9	11.25	1.88	0.74
Dermis	1900	1.4	1.4	32	4	237	213	0.72	0.78	5.2	0.9	0.3

3.4. Boundary Conditions

It is assumed that an index matching cream has been applied onto the surface between the optical probe and the skin. Then, the internal-reflection at the interface of the skin and the probe can be ignored. Indeed, if there were no index matching cream applied, any photon coming from within the tissue and reaching the interface at an angle greater than the critical angle will be reflected back into the tissue. The critical angle is defined as $\theta_c = \arcsin(1/n_{epi})$ where n_{epi} is the refractive index of the epidermis. Moreover, the skin surface and the interfaces between the skin layers are inherently rough and should be accounted for in simulations to understand their influence on the distribution of excitation and fluorescence light in skin [37]. However, for the sake of simplicity, they are assumed to be optically smooth and plane parallel as commonly done in the literature [37].

Finally, the incident pulse at $z = 0.0$ is assumed to be Gaussian with a peak intensity I_0 at time $t = t_c$ and pulse width t_p and is expressed as,

$$I_i(t) = I_0 \exp\left[-4\ln(2)\left(\frac{t - t_c}{t_p}\right)^2\right] \tag{4}$$

The pulse width t_p was chosen to be 1.0 ns, $t_c/t_p = 3$, and $I_0 = 10.0$ W/m^2sr. The intensity is typical of a collimated beam from a pulsed LED with a peak power of 1.0 mW shining on area of about 1.0 cm^2.

3.5. Method of Solution

Finally, Equations (1) and (2) are solved successively using the modified method of characteristics [24]. The reader is referred to [24,25] for a detailed description of the solution procedure. Moreover, the integrals present in Equations (1) and (2) are computed using a quadrature scheme. It is a combination of two Gaussian quadratures consisting of 24 directions along with the associated weights and has been successfully used in radiation transport calculations for strongly forward scattering media [38]. Finally, the time-resolved hemispherical reflectance and the autofluorescence emerging from the skin are computed as follows and plotted as a function of time,

$$R(t) = 2\pi \int_{\pi/2}^{\pi} I_{\lambda_x}(0, \theta, t) \cos\theta \sin\theta d\theta \quad \text{and} \quad F(t) = 2\pi \int_{\pi/2}^{\pi} I_{\lambda_F}(0, \theta, t) \cos\theta \sin\theta d\theta \tag{5}$$

4. RESULTS AND DISCUSSION

Two cases of time-resolved fluorescence from skin are simulated. The first simulates time-resolved autofluorescence of human skin exposed to a collimated pulse of light. The optical and radiation characteristics for this simulation are given in Table 1. A grid size of $N_z = 201$ resulting in a numerically converged solution was used. In the second case, the time-resolved fluorescence from skin with an implanted fluorescence sensor for glucose sensing was simulated. The optical and radiation characteristics for this simulation are listed in Table 2. Here, a grid size of $N_z = 206$ resulting in a numerically converged solution was used.

4.1. Time-Resolved Autofluorescence of Human Skin

Time-resolved Hemispherical Reflectance and Fluorescence

Figure 2 shows the normalized hemispherical reflectance R(t) and autofluorescence F(t) from skin exposed to the excitation pulse described by Equation (4). Both were normalized by dividing their values by their maxima estimated at 1.35 W/m^2 and 4.22 $\times 10^{-3}$ W/m^2, respectively. Figure 2 indicates that the shape of the normalized hemispherical reflectance is identical to the shape of the excitation pulse. The temporal profile as well as the magnitude of the reflectance depends on the separation between the detector and the source. As the distance between the source and the detector increases, the depth of skin probed increases. Moreover, the path length traveled by the photons increases and as a result the temporal profile of the reflectance is broadened compared to the incident pulse. However, the present study makes use of a wide beam illumination and reflectance is measured at the center of this beam. Thus, the detected reflectance represents an integrated contribution of the reflectances from all source-detector separations varying from zero to infinity. However, the major contribution to the diffuse reflectance is from photons back-scattered by the topmost layers of the tissue. Since the path length traveled by these photons through the skin is negligible, the temporal profile of the reflectance does not undergo any broadening and is identical to the incident pulse. Unlike the reflectance, the hemispherical autofluorescence is temporally broadened due to the fluorescence lifetimes of the fluorophores.
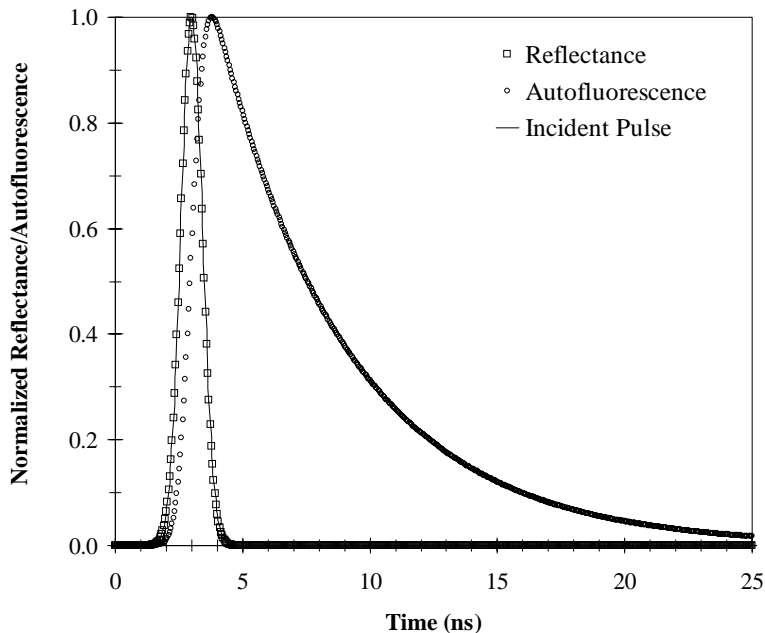

Figure 2. Normalized hemispherical reflectance and autofluorescence from skin irradiated by a collimated nanosecond pulse as a function of time.

Retrieval of Fluorescence Lifetimes

In time-resolved fluorescence experiments, one recovers the fluorescence lifetimes from the normalized time-resolved fluorescence decay by deconvoluting the Instrument Response Function or IRF from the measured fluorescence decay. The IRF represents the response of the instrument to a fluorophore with zero lifetime. As performed experimentally, a model decay can be fit to the numerical hemispherical fluorescence decay using the incident pulse as the IRF. The software Fluofit [26, 27] programmed in Matlab was used to fit the simulated fluorescence decay to a bi-exponential model of the form,

$$F(t) = A_1 \exp(-t/\tau_1) + A_2 \exp(-t/\tau_2) \tag{6}$$

The program made use of a least squares fit and the Nelder-Meade simplex algorithm for optimization. The recovered parameters τ_1, τ_2, A_1 and A_2 were 0.2 ns, 5.2 ns, 0.04 and 0.96 respectively. While the second lifetime of 5.2 ns corresponds to the intrinsic lifetime of collagen located in the dermis, the intrinsic lifetime of NADH located in the epidermis and set at 1.5 ns was not recovered. This could be due to fact that the contribution of NADH to the fluorescence was very minimal, making it numerically difficult to recover its lifetime. Moreover, it was found that the fluorescence lifetime of NADH varied from one run to another and was also sensitive to the version of Matlab used (6.5 and 7.0).

4.2. Reflectance and Autofluorescence from the two-layer skin model

As described earlier, a two-layer skin model was also developed by averaging the properties of the five-layer skin model. The reflectance and autofluorescence from this skin model was then computed. The peak values of reflectance and autofluorescence for the two-layer skin model were $1.25 \ W/m^2$ and $3.35 \times 10^{-3} \ W/m^2$ respectively representing a decrease of 7% and 21% from the five-layer skin model. On the other hand the recovered lifetime 5.18 ns was close to the intrinsic lifetime of 5.2 ns of collagen used in the simulations, similar to the five-layer skin model. However, the fluorescence lifetime of NADH could not be recovered. The two layer model was chosen for the feasibility analysis of the sensor for two reasons, (i) the magnitude of the fluorescence signal does not affect the recovered fluorescence lifetimes, (ii) computational time is reduced compared with the five-layer skin model. This confirms the advantage of time-resolved fluorescence measurements and contrast with steady-state measurements which are dependent on the magnitude of the intensity and thus are sensitive to the skin model used.

4.3. Evaluation of an Embedded Sensor under the Epidermis for Biomedical Diagnostics

There has been a rising interest in the use of implanted sensors for non-invasively monitoring concentrations of various analytes such as glucose in the human body. Several studies have reported the *steady-state* intensity and spatial distribution of fluorescence emission from hypothetical sensors under the skin using the Monte Carlo method [2, 3, 39]. In the present study, simulations of *time-resolved* fluorescence from sensors embedded between the epidermis and the papillary dermis are presented for the first time.

In the present simulations, the mean fluorescence lifetime of the fluorophore present in the sensor layer is varied from 11.25 ns to 12 ns in response to a change in the concentration of glucose in the interstitial fluid from 5mM to 20 mM [5]. Figure 3 shows the time-resolved fluorescence of skin with this implanted sensor for these two glucose concentrations. Once again, Fluofit [26, 27] was used to recover the fluorescence lifetimes from these decays. For a glucose concentration of 5mM equivalent to 90 mg/dL, the recovered lifetimes were 0.0285 ns, 5.3 ns, and 11.50 ns, and their corresponding amplitudes were 0.57, 0.20, and 0.23 respectively. In contrast, the fluorescence lifetimes of the fluorophores used in the simulations were 1.5 ns, 5.2 ns, and 11.25 ns. Moreover, for a glucose concentration of 20 mM, the recovered lifetimes were 0.0288 ns, 5.1 ns, and 12.0 ns with the corresponding amplitudes being 0.33, 0.32, and 0.35 respectively. The lifetimes of the fluorophores used in the simulations were 1.5 ns, 5.2 ns, and 12.0 ns. For both cases, while the fluorescence lifetimes for collagen and the glucose sensor were recovered within 2.5% of their values used in the simulations, the lifetime of NADH in the epidermis could not be recovered. In comparison, the change in the mean fluorescence lifetime of the fluorophore was 6.7% for glucose concentration varying from 5mM to 20mM. These results indicate that it is possible to measure glucose concentrations *in-vivo* using a time-resolved fluorescence sensor. It should however be noted that these simulations represent ideal conditions which might not be achievable in actual experiments.
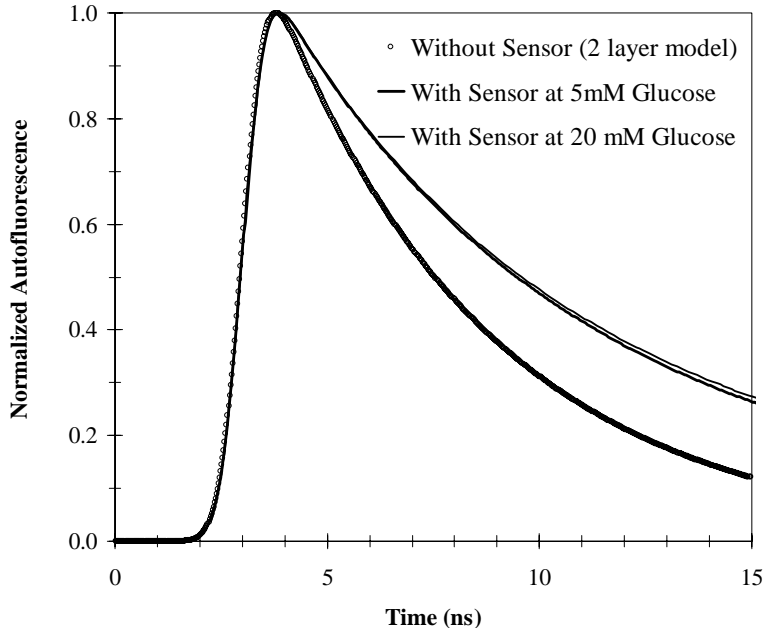
Figure 3. Normalized hemispherical fluorescence from skin with an implanted glucose sensor and irradiated by a collimated nanosecond pulse as a function of time.

For example the morphology of skin changes from one person to another. This is especially important in diabetic patients whose skin may thicken as a result of the disease [40]. Moreover, the unavoidable noise in experimental data may affect the recovered lifetimes. However, these effects can be studied by varying the optical properties of tissue used in the present simulations as well as adding simulated noise to the hemispherical fluorescence obtained numerically. Furthermore, various other excitation and detection geometries can be tested.

5. CONCLUSIONS

In this paper, we presented simulations of time-resolved fluorescence from skin and their applications for designing implantable sensors for glucose monitoring. First, a five-layered skin fluorescence model was developed based on various data reported in literature. Second, the time-resolved fluorescence from human skin obtained by solving the radiative transfer equation was presented. Then, an attempt was made to recover the fluorescence lifetimes of the fluorophores present in the skin. It was found that the fluorescent lifetime of collagen in the dermis could be recovered accurately while the lifetime of NADH in the epidermis used in the simulations could not be recovered. This was attributed to the fact that the contribution of NADH to the overall fluorescence was minimal. Moreover, a simplified two-layer model of the skin was developed by averaging the properties of the five layered skin model. In spite of the peak values of the fluorescence from the five-layer and two-layer model being different, it had no effect on the recovered fluorescence lifetime of collagen. This confirms that, unlike steady-state measurements, time-resolved measurements do not depend on the magnitude of the intensity, but only on the temporal shape of the fluorescence decay. Finally, the feasibility of a sensor layer implanted between the epidermis and the dermis was studied. Again, the lifetime of NADH could not be recovered while the lifetime of collagen and the sensor could be recovered accurately within 2.5% of the actual lifetimes used in the simulations. The results indicated that it would be possible to measure glucose concentrations non-invasively using a time-resolved fluorescence sensor. However, the present study does not account for conditions such as varying skin morphologies and noise encountered in actual experiments which might make it harder to retrieve the fluorescence lifetimes accurately. Future studies will need to account for these in the simulations. The simulations in the present study are of particular interest for designing implantable non-invasive fluorescence sensors, pharmacokinetics,

and non-invasive diagnosis of various diseases which alter the autofluorescence properties of human skin. Further studies of time-resolved autofluorescence from skin could incorporate (i) more complex excitation and detection geometries (ii) more realistic skin morphology (iii) and the presence of multiple fluorophores with complex spatial distributions (iv) account for noise as encountered in experimental data.

6. ACKNOWLEDGEMENTS

REFERENCES

1. R. Richards-Kortum and E. Sevick-Muraca, "Quantitative optical spectroscopy for tissue diagnostics," *Annual Review of Physical Chemistry* **47**, pp. 555–606, 1996.
2. M. McShane, S. Rastegar, and G. Cote, "Fluorescence-based implantable biosensors: Monte carlo modeling for optical probe design," *Engineering in Medicine and Biology Society,Proceedings of the 20th Annual International Conference of the IEEE* **4**(29), pp. 1799–1802, 1998.
3. M. McShane, S. Rastegar, M. Pishko, and G. Cote, "Monte carlo modeling for implantable fluorescent analyte sensors," *Biomedical Engineering, IEEE Transactions on* **47**(5), pp. 624–632, 2000.
4. D. P. O'Neal, M. J. McShane, M. V. Pishko, and G. L. Cote, "Implantable biosensors: analysis of fluorescent light propagation through skin," *Proceedings of the SPIE* **4263**, pp. 20–24, 2001.
5. D. N. and L. J.R., "Evaluation of two synthetic glucose probes for fluorescence-lifetime-based sensing," *Analytical Biochemistry* **294**(2), pp. 154–160, 2001.
6. M. Keijzer, R. Richards-Kortum, S. Jacques, and M. Feld, "Fluorescence spectroscopy of turbid media: Autofluorescence of the human aorta," *Applied Optics* **28**, pp. 4286–4292, 1989.
7. I. V. Meglinski and D. Y. Churmakov, "A novel Monte Carlo method for the optical diagnostics of skin," *Proceedings of the SPIE* **5141**, pp. 133–141, 2003.
8. I. V. Meglinski, "Monte Carlo method in optical diagnostics of skin and skin tissues," *Proceedings of the SPIE* **5254**, pp. 30–43, 2003.
9. H. Zeng, C. E. MacAulay, B. Palcic, and D. I. McLean, "Monte Carlo modeling of tissue autofluorescence measurement and imaging," *Proceedings of the SPIE* **2135**, pp. 94–104, 1994.
10. M. F. Modest, *Radiative Heat Transfer*, Academic Press, San Diego, CA, 2002.
11. K. Vishwanath, B. Pogue, and M.-A. Mycek, "Quantitative fluorescence lifetime spectroscopy in turbid media: comparison of theoretical, experimental and computational methods," *Physics in Medicine and Biology* **47**, pp. 3387–3405, 2002.
12. M. A. Mycek, K. Vishwanath, B. W. Pogue, K. T. Schomacker, and N. S. Nishioka, "Simulations of time-resolved fluorescence in multi-layered biological tissues: Applications to clinical data modeling," *Proceedings of the SPIE* **4958**, pp. 51–59, 2003.
13. K. Vishwanath and M.-A. Mycek, "Do fluorescence decays remitted from tissues accurately reflect intrinsic fluorophore lifetimes?," *Optics Letters* **29**(13), pp. 1512–1514, 2004.
14. M. S. Patterson and B. W. Pogue, "Mathematical model for time-resolved and frequency-domain fluorescence spectroscopy in biological tissues," *Applied Optics* **33**(10), pp. 1963–1974, 1994.
15. M. A. O'Leary, D. A. Boas, X. D. Li, B. Chance, and A. G. Yodh, "Fluorescence lifetime imaging in turbid media," *Optics Letters* **21**(2), pp. 158–160, 1996.
16. E. M. Sevick-Muraca and D. Y. Paithankar, "Imaging of fluorescence yield and lifetime from multiply scattered light re-emitted from random media," *Proceedings of the SPIE* **2980**, pp. 303–318, 1997.
17. D. Y. Paithankar, A. U. Chen, B. W. Pogue, M. S. Patterson, and E. M. Sevick-Muraca, "Imaging of fluorescent yield and lifetime from multiply scattered light reemitted from random media," *Applied Optics* **36**(10), pp. 2260–2272, 1997.
18. A. H. Hielscher, R. E. Alcouffe, and R. L. Barbour, "Comparison of finite-difference transport and diffusion calculations for photon migration in homogeneous and heterogeneous tissues," *Physics in Medicine and Biology* **43**, pp. 1285–1302, 1998.

19. R. Elaloufi, R. Carminati, and J. J. Greffet, "Time-dependent transport through scattering media: from radiative transfer to diffusion," *Journal of Optics A: Pure And Applied Optics* **4**(5), pp. S103–S108, 2002.

20. Z. Guo and K. Kim, "Ultrafast-laser-radiation transfer in heterogeneous tissues with the discrete-ordinates method," *Applied Optics* **42**, pp. 2897–2905, 2003.

21. T. Spott and L. O. Svaasand, "Collimated light sources in the diffusion approximation," *Applied Optics* **39**, pp. 6453–6465, 2000.

22. G. Yoon, S. A. Prahl, and A. J. Welch, "Accuracies of the diffusion approximation and its similarity relations for laser irradiated biological media," *Applied Optics* **28**, pp. 2250–2255, 1989.

23. N. Evans, L. Gnudi, O. Rolinski, D. Birch, and J. Pickup, "Glucose-dependent changes in NAD(P)H-related fluorescence lifetime of adipocytes and fibroblasts in vitro: Potential for non-invasive glucose sensing in diabetes mellitus," *Journal of Photochemistry and Photobiology B: Biology* **80**(2), pp. 122–129, 2005.

24. K. Katika and L. Pilon, "Modified method of characteristics in transient radiative transfer," *Journal of Quantitative Spectroscopic and Radiative Transfer* **98**, pp. 220–237, 2005.

25. K. Katika and L. Pilon, "Steady-state directional diffuse reflectance and fluorescence of human skin," *Applied Optics, in review* .

26. J. Enderlein and R. Erdmann, "Fast fitting of multi-exponential decay curves," *Optics Communications* **134(1-6)**, pp. 371–378, 1997.

27. "Fluofit - a matlab package for fitting multiexponential fluorescence decay curves." http://www.fz-juelich.de/ibi/ibi-1/enderlein/joerg/fluo/fluo.html, last accessed, December 22, 2005.

28. I. V. Meglinski and S. J. Matcher, "Monte Carlo method in optical diagnostics of skin and skin tissues," *Proceedings of the SPIE* **4241**, pp. 78–87, 2001.

29. A. Krishnaswamy and G. V. G. Baranoski, "A study on skin optics," *Technical Report CS-2004–01, School of Computer Science, University of Waterloo* , 2004.

30. V. Tuchin, ed., *Tissue Optics:Light Scattering Methods and Instruments for Medical Diagnosis*, SPIE Press, 2000.

31. H. Quan and Z. Guo, "Fast 3-D optical imaging with transient fluorescence signals," *Optics Express* **12**(3), pp. 449–457, 2004.

32. H. Zeng, C. MacAulay, D. I. McLean, and B. Palcic, "Reconstruction of in vivo skin autofluorescence spectrum from microscopic properties by Monte Carlo simulation," *Journal of Photochemistry and Photobiology B: Biology* **38**, pp. 234–240, 1997.

33. D. Y. Churmakov, I. V. Meglinski, S. A. Piletsky, and D. A. Greenhalgh, "Skin fluorescence model based on the Monte Carlo technique," *Proceedings of the SPIE* **5068**, pp. 326–333, 2003.

34. R. Gillies, G. Zonios, R. R. Anderson, and N. Kollias, "Fluorescence excitation spectroscopy provides information about human skin in vivo," *Journal of Investigative Dermatology* **115**(4), pp. 704–707, 2000.

35. K. Konig and I. Riemann, "High-resolution multiphoton tomography of human skin with subcellular spatial resolution and picosecond time resolution," *Journal of Biomedical Optics* **8**(3), pp. 432–439, 2003.

36. G. L. Cote, M. D. Fox, and R. B. Northrop, "Noninvasive optical polarimetric glucose sensing using a true phase measurement technique," *IEEE Transactions on Biomedical Engineering* **39**(7), pp. 752–756, 1992.

37. J. Q. Lu, X.-H. Hu, and K. Dong, "Modeling of the rough-interface effect on a converging light beam propagating in a skin tissue phantom," *Applied Optics* **39**, pp. 5890–5897, 2000.

38. D. Baillis, L. Pilon, H. Randrianalisoa, R. Gomez, and R. Viskanta, "Measurements of radiation characteristics of fused quartz containing bubbles," *Journal of the Optical Society of America A* **21**, pp. 149–159, 2004.

39. D. Y. Churmakov, I. V. Meglinski, and D. A. Greenhalgh, "Amending of fluorescence sensor signal localization in human skin by matching of the refractive index," *Journal of Biomedical Optics* **9**, pp. 339–346, 2004.

40. A. Huntley and R. Drugge, "Diabetes in skin disease. the electronic textbook of dermatology." http://www.telemedicine.org/dm/dmupdate.htm, last accessed, September 5, 2005.